Realistic macronova models with detailed elemental opacities and thermalized r-process heating

Ryan T. Wollaeger

Los Alamos National Laboratory

LA-UR-17-20220

January 18, 2017

Collaborators

- Oleg Korobkin[1],
- Christopher J. Fontes[1],
- Christopher L. Fryer[1],
- Aimee L. Hungerford[1],
- Stephan K. Rosswog[2],
- Wesley P. Even[1],
- Allan B. Wollaber[1]
- Daniel R. van Rossum[3]

[1] *Los Alamos National Laboratory*
[2] *The Oskar Klein Centre, Department of Astronomy, Stockholm University*
[3] *Flash Center for Computational Science, University of Chicago*

Abstract

Macronovae (also known as kilonovae) are elusive infrared/optical counterparts to binary neutron star mergers, powered by radioactive decay of freshly synthesized heavy elements in various outflows from the mergers. Search for macronovae is hindered by many uncertainties, such as morphology of the ejecta, opacities of heavy elemental plasma, ejecta composition, nuclear properties, radioactive heat thermalization and so on.
In this study, we address some of these uncertainties with our state-of-the art opacities and radiative transfer simulations. We present several macronova models with increasing levels of realism, gauging the impact of different physics on the light curves and spectra. Our most complex models feature 2D axisymmetric ejecta morphology with wind and dynamical ejecta components, detailed elemental opacities, detailed r-process heating with thermalization fractions, and simplified time-depenendent gamma-ray transfer. For the radiative transfer, we use the Monte Carlo code SuperNu, and detailed LTE opacities tabulated from the LANL suite of atomic physics codes. r-process heating is computed with the WinNet nucleosynthesis network, and we integrate our spectra over the grizyJHK filters, suitable for survey facilities such as LSST and VISTA.
Our light curves generally peak on the order of a few days in the IR bands, with some models having a blue transient corresponding to the wind. Absolute peak K-band magnitudes range from -11 to -15, with more realistic models ranging from -14 to -15. Similarly to previous studies, for the most realistic 2D models we find that the bluer transient from the wind is extremely sensitive to lanthanide curtaining from the dynamical ejecta. We discuss macronovae observability, diagnostics and current limitations in our models.

Table of Contents

Binary pulsars

- Most massive stars are believed to be in binaries. (Kiminki et al 2007, Sana et al 2012, Kobulnicky et al 2014)
- These binary stars can produce binary pulser systems and these are observed. (Martinez et al 2015, Özel et al 2016, Lazarus et al 2016)
- Population synthesis models predict the rate of binary systems to $\sim 0.01 - 100$ per Myr in a Milky Way massed galaxy, with t_{merger} from < 10 Myr to the age of the universe. (Fryer et al 1999, Dominik et al 2012)

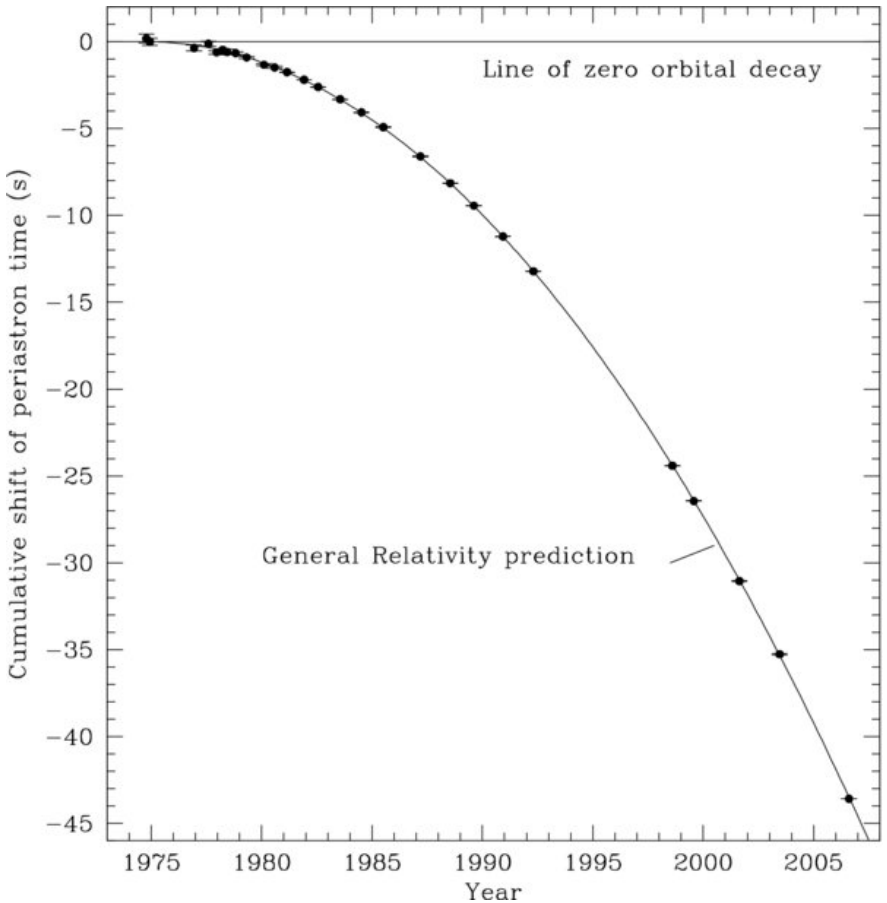

Weisberg et al (2010)

Neutron star mergers

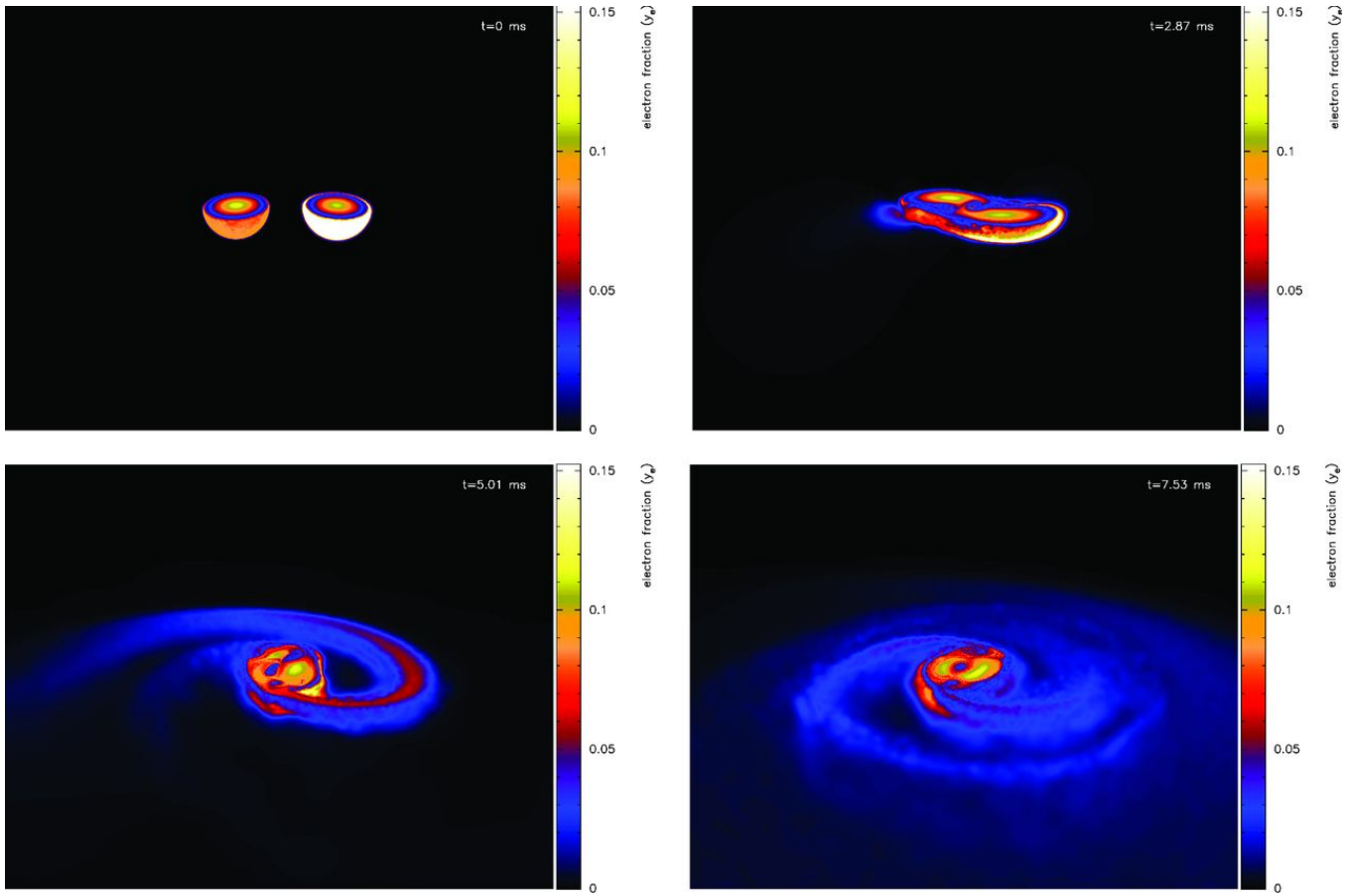

Rosswog et al (2013)

Dynamical ejecta and wind outflows

- Types of NSM outflows:
  - dynamical ejecta
    ($10^{-4} < M < 0.04\ \mathrm{M}_\odot$,
    $0.04 < Y_e < 0.2$,
    $v \sim 0.1 - 0.3c$),
  - ν- and magnetically-driven wind from HMNS
    ($10^{-5} < M < 5 \times 10^{-3}\ \mathrm{M}_\odot$,
    $0.25 < Ye < 0.5$,
    $v \sim 0.06 - 0.1c$),
  - accretion disc wind
    ($10^{-4} < M < 0.05\ \mathrm{M}_\odot$,
    $0.15 < Y_e < 0.3$, $v \sim 0.08c$),
  - ultrarelativistic GRB jet.

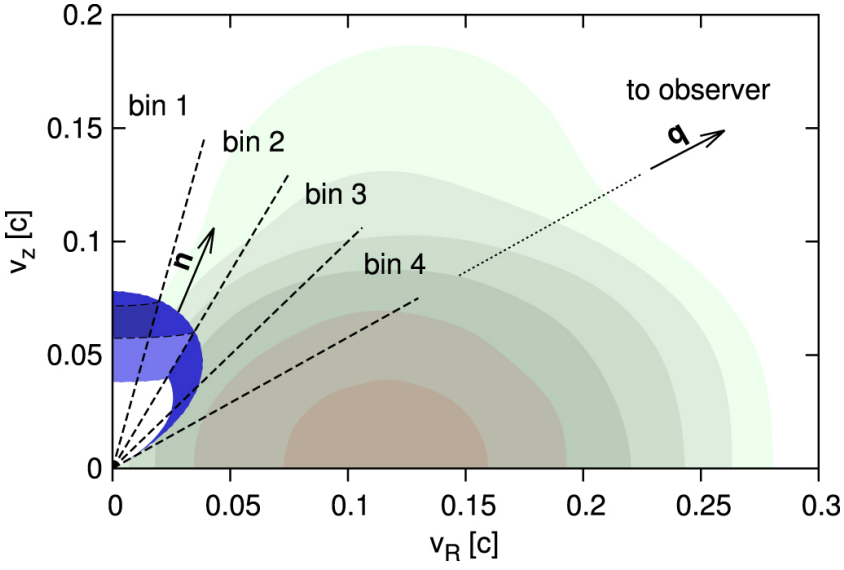

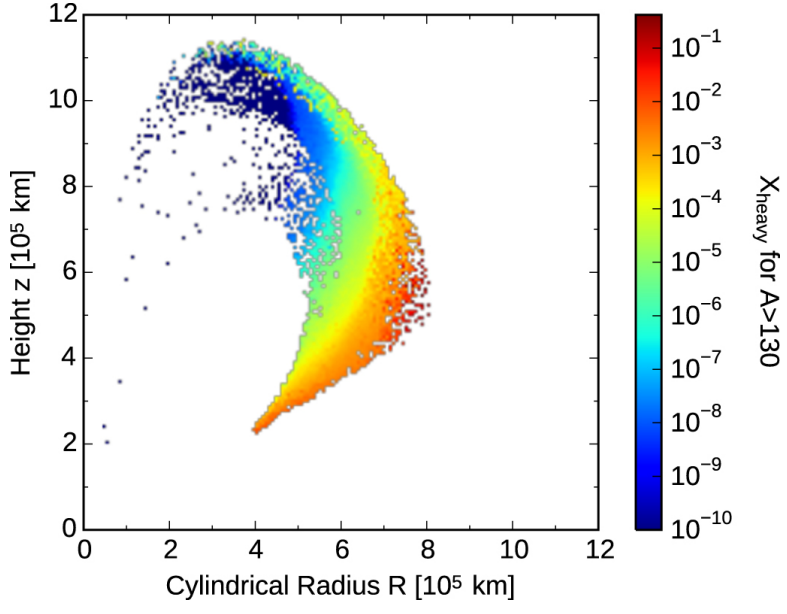

Martin et al (2015)

Sites of r-process

- Some observational evidence points to rare, prolific sites:
  - robust pattern of the main r-process in metal poor stars (Sneden et al 2008),
  - r-process enriched galaxy (Ji et al. 2016),
  - lack of live ^{244}Pu in the deep see fossil records over the last 25 Myr.

    (Wallner et al 2015)

- However:
  - population synthesis result in low rates (Cote et al, 2016),
  - ISM mixing is not sufficiently inhomogeneous (Argast et al 2004).

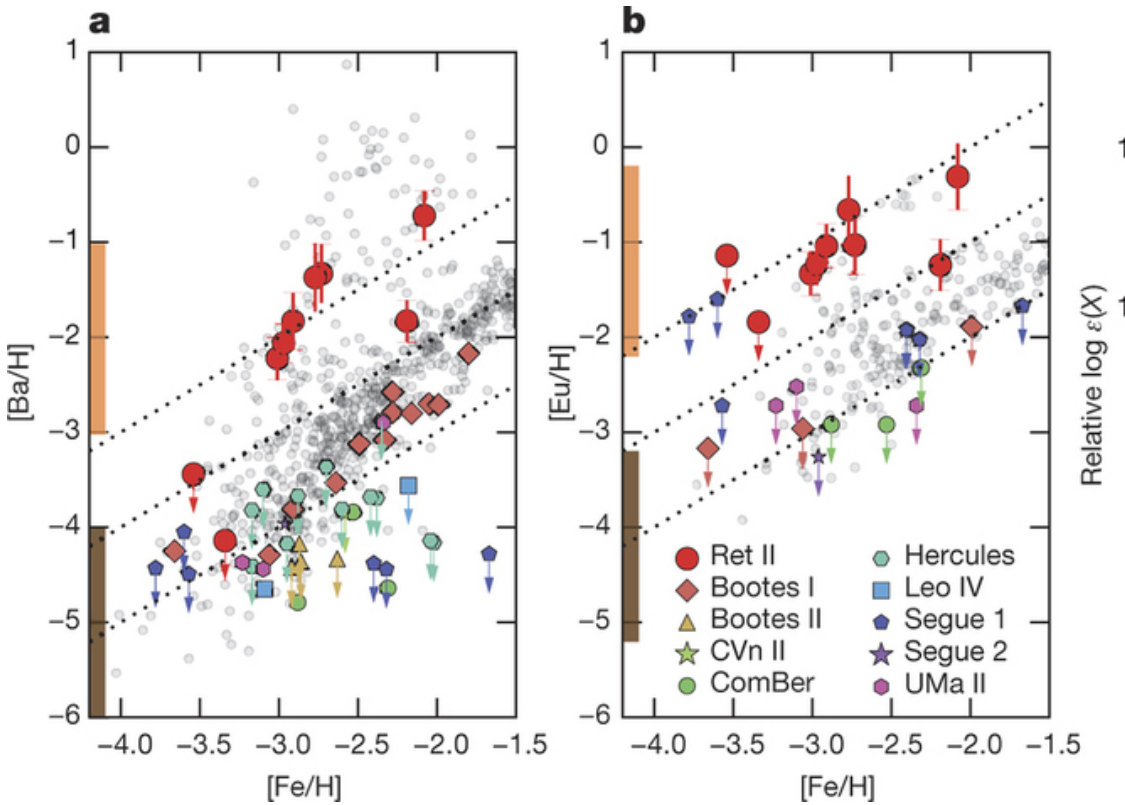

Ji et al (2016)

Macronovae (or Kilonovae)

- Radioactive r-process abundances power optical-IR transient.

  (Li and Paczyński 1998, Review: Metzger 2016)

- Unlike GRB emission which is beamed, the macronova emission should be more or less isotropic.

  (Fong et al 2015)

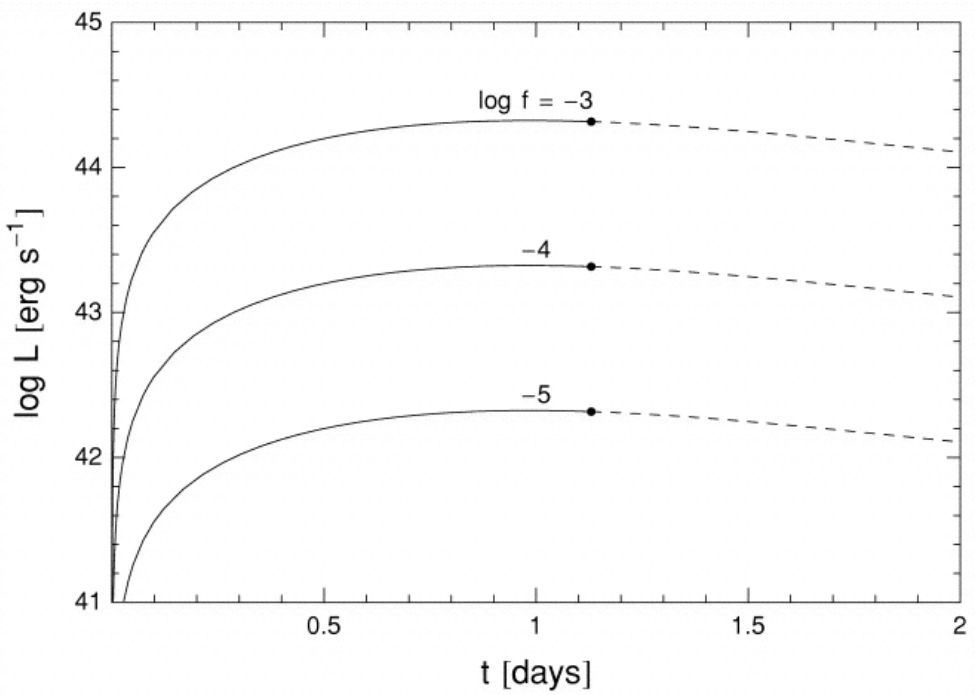

Li and Paczyński (1998)

Macronova candidates

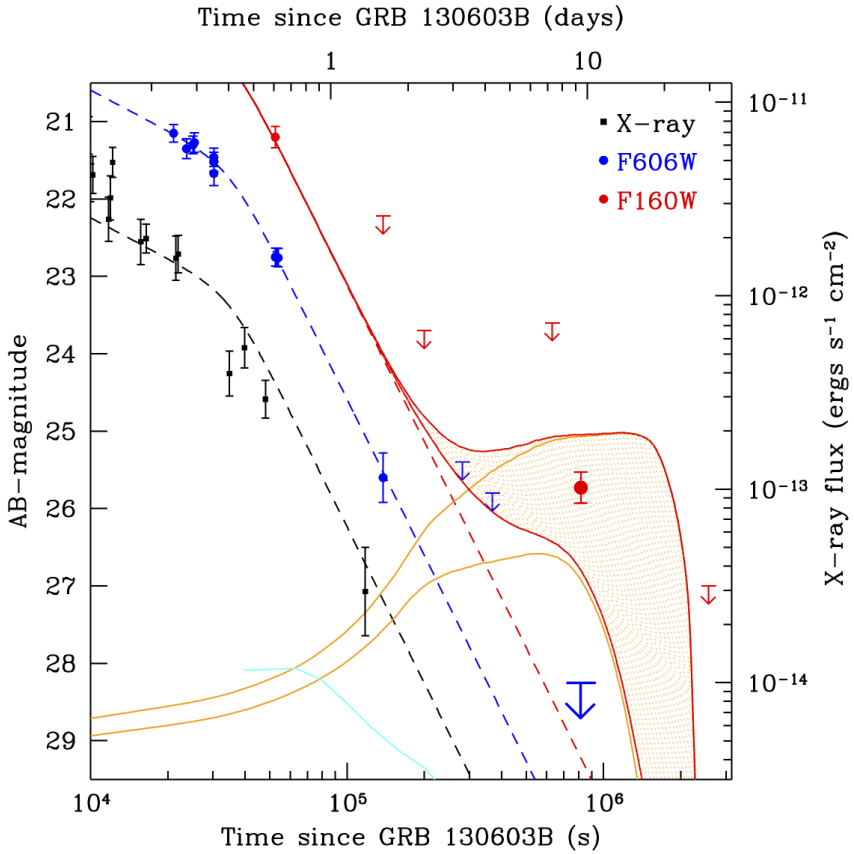

Tanvir et al (2013)

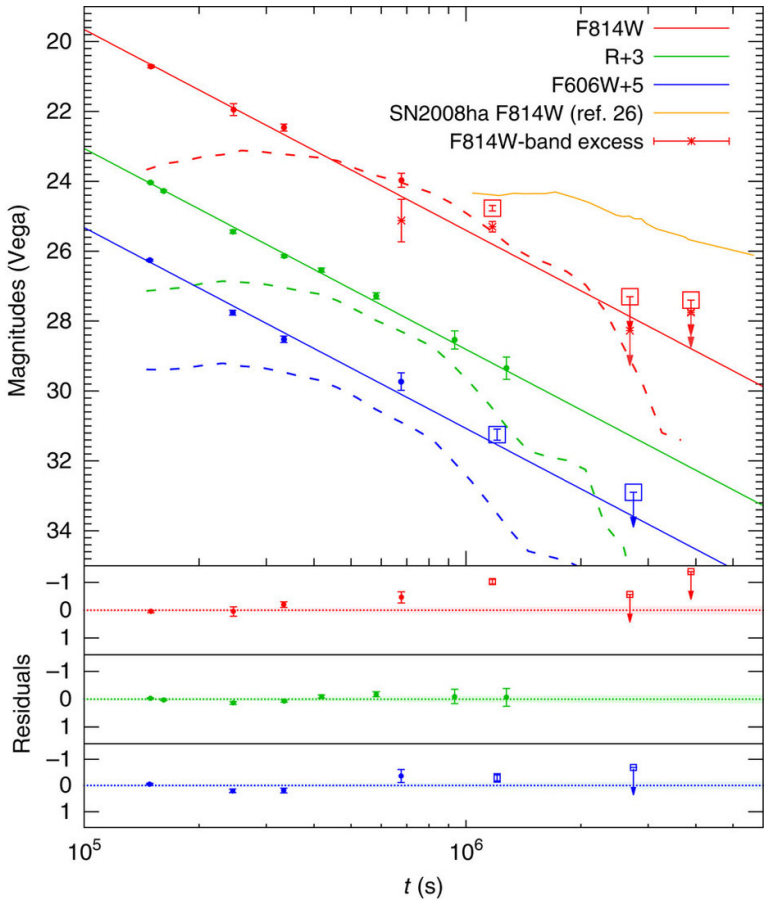

Yang et al (2015)

Macronova candidates

- Non-detection for GRB 150101B:

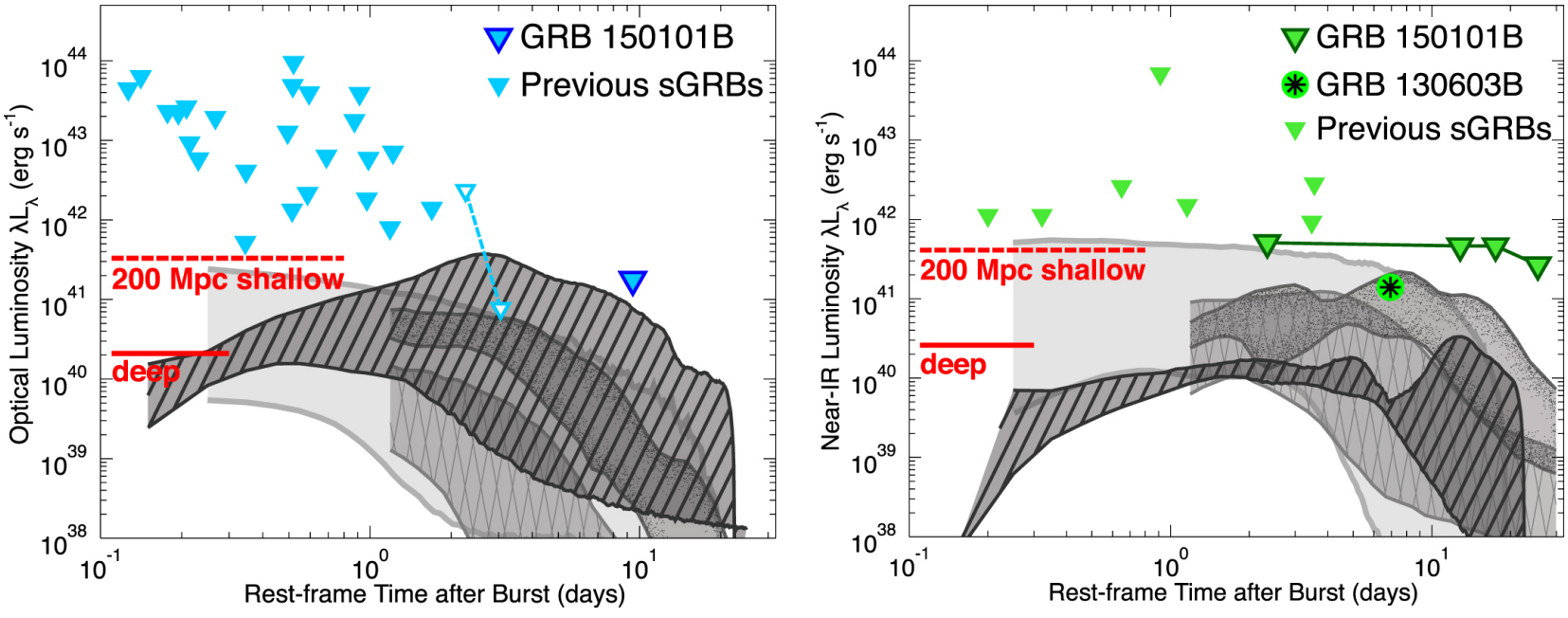

Fong et al (2016)

Numerical methods

Radiative transfer

- Radiative transfer is performed with `SuperNu`.
- Radiative transfer is:
  - multigroup,
  - multidimensional,
  - LTE,
  - Monte Carlo (IMC-DDMC),
  - for O(V/c) homologous outflow.

(Wollaeger et al 2013, Wollaeger and van Rossum 2014)

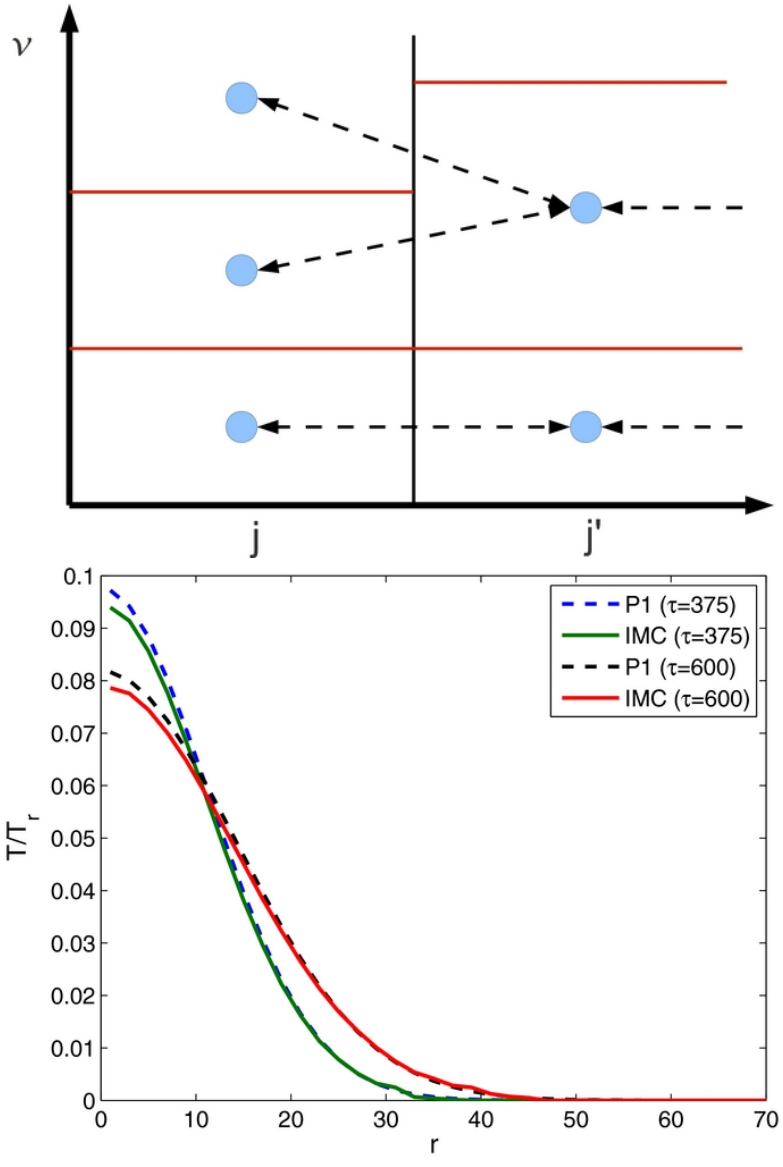

(Wollaeger et al 2013)

Opacity

- Opacities are calculated from the LANL suite of atomic physics codes.

  (Fontes et al 2015b)

- Narrow lines are resolved by artificially broadening lines in the opacity calculation.
  - $\Delta V/c \sim \Delta\lambda/\lambda \sim 0.01$

  (Fontes et al 2015)

- All opacity tables range from T =116 K (0.01 eV) to 58000 K (5 eV), and $\rho = 10^{-20}$ g/cc to 10^{-4} g/cc.

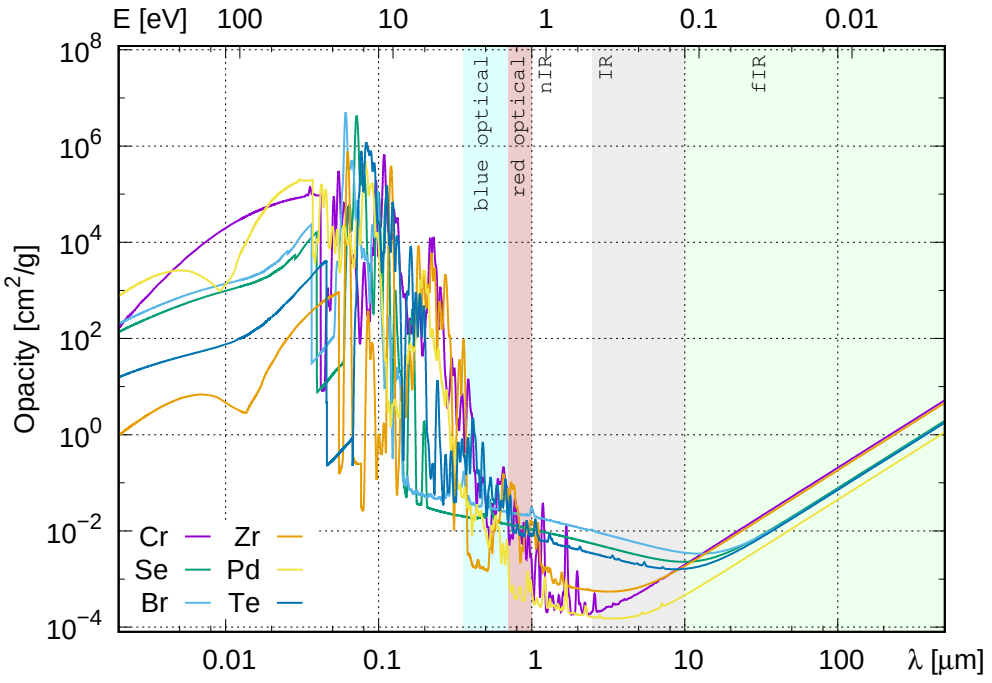

LTE opacity at $T = 5800$ K and $\rho = 10^{-13}$ g/cc.

Models and results

Models

- Morphology: 1D semi-analytic, 2D axisymmetric-averaged Rosswog et al (2013) models A-D, or spherical wind + dyn. ej. from Rosswog et al (2013).
- Composition: grey (opacity), Sm dyn. ej., Sm dyn. ej.+(Se,Br,Te,Pd,Zr,Cr) wind, or mixed dyn. ej.+ low (or high) latitude mixed wind.
- r-process heating: simple power law $\sim 1/t^{1.3}$ (Korobkin et al 2012), WinNet result+thermalization fractions (Winteler 2011 PhD thesis, Barnes et al 2016), or WinNet result+thermalization fractions (excluding γ-ray source)+grey MC $\sigma_\gamma = .1$ cm^2/g transport for γ-ray deposition.

Models

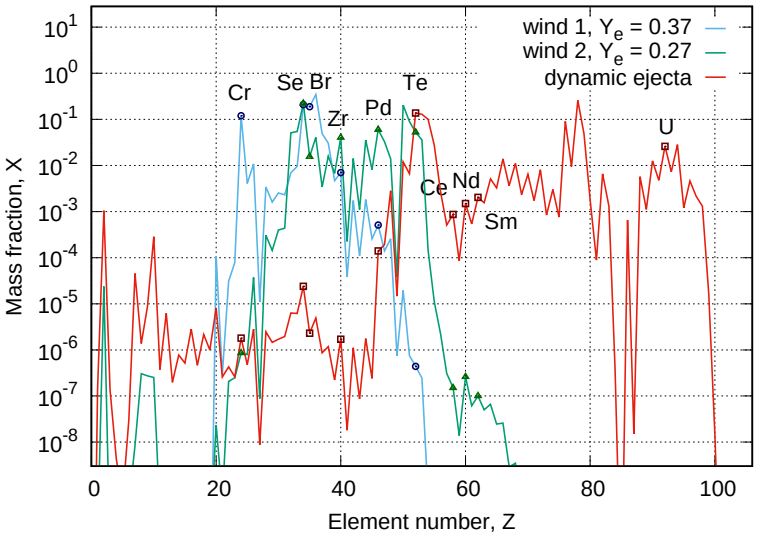

Elem.	Wind 1	Wind 2	Dynamical ejecta
$_{24}$Cr	0.120	8.6×10^{-7}	1.8×10^{-6}
$_{34}$Se	0.208	0.222	2.4×10^{-5}
$_{35}$Br	0.188	0.0156	2.3×10^{-6}
$_{40}$Zr	0.007	0.0405	1.7×10^{-6}
$_{46}$Pd	5.1×10^{-4}	0.0598	1.4×10^{-4}
$_{52}$Te	4.4×10^{-7}	0.0523	0.137
$_{58}$Ce	$< 10^{-20}$	1.5×10^{-7}	0.00087
$_{60}$Nd	$< 10^{-20}$	2.6×10^{-7}	0.00149
$_{62}$Sm	$< 10^{-20}$	1.0×10^{-7}	0.00203
$_{92}$U	$< 10^{-20}$	$< 10^{-20}$	0.026

(Rosswog et al 2014, Perego et al 2014)

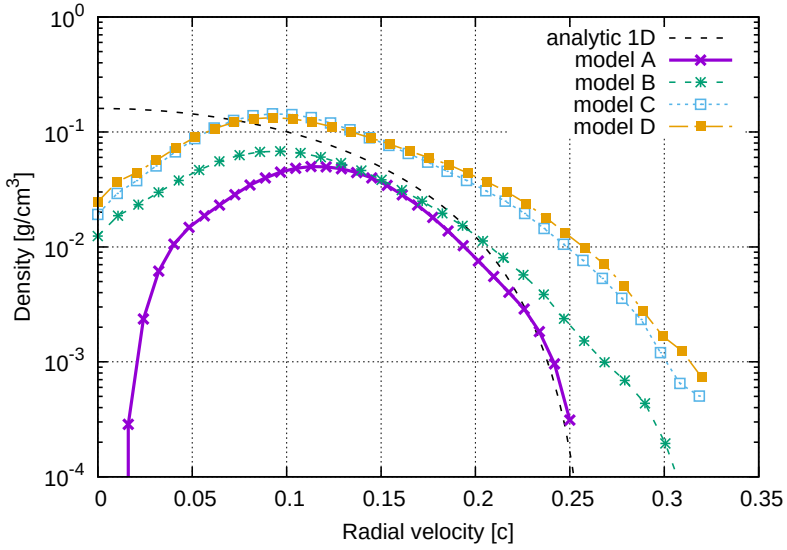

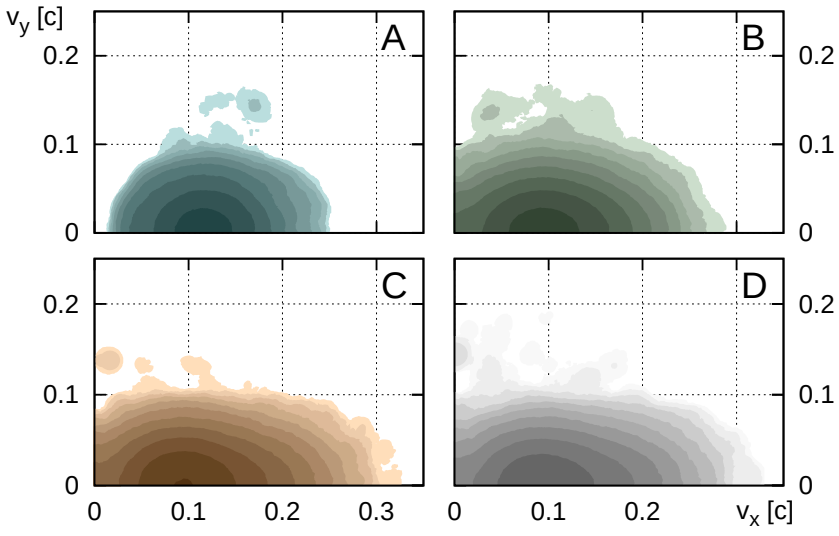

(Rosswog et al 2013)

Semi-analytic (1D)

- Ansatz based on exact solution for spherically symmetric homologous outflow with $\Gamma = 4/3$:

$$\rho(t, r) = \rho_0 \left(\frac{t_0}{t}\right)^3 \left(1 - \left(\frac{rt}{V_{\max}}\right)^2\right)^3$$

- Source ($\epsilon_{th} = 0.25$):

$$\dot{\epsilon}(t) = \epsilon_{th} \cdot 2 \times 10^{10} t_d^{-1.3} \frac{\text{erg}}{\text{g} \cdot \text{s}}$$

- Mass, velocity, and grey absorption opacity are varied:
  - $M \in \{0.1, 0.01, 0.001\}\ \text{M}_\odot$,
  - $V_{\max} \in \{0.1, 0.2, 0.3\}\ c$,
  - $\kappa \in \{1, 10, 100, 1000\}\ \text{cm}^2/\text{g}$.

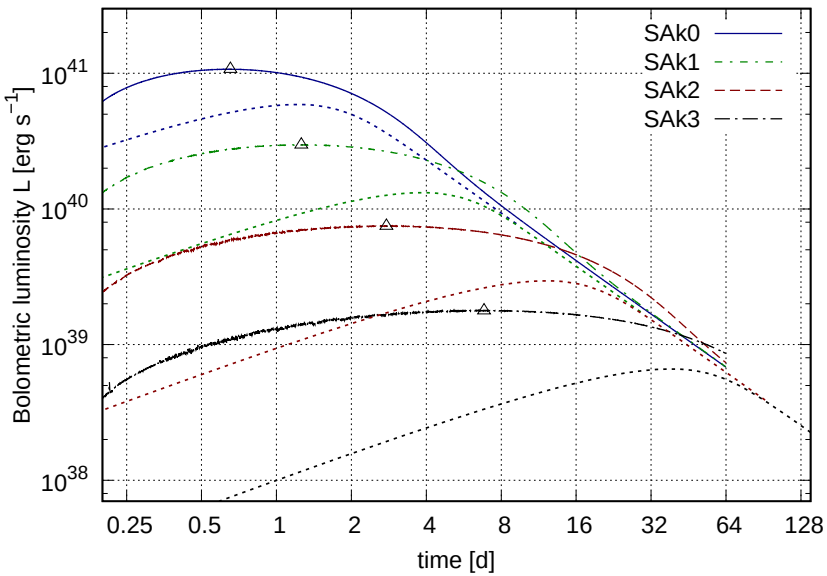

Semi-analytic (1D)

- Scaling fits for broad-band light curve peaks:

$$m_g = -12.05 - 1.13 \log_{10} M_2 - 1.28 \log_{10} v_{-1} + 2.65 \log_{10} \kappa_{10}$$
$$m_r = -12.38 - 1.01 \log_{10} M_2 - 1.60 \log_{10} v_{-1} + 2.27 \log_{10} \kappa_{10}$$
$$m_i = -12.67 - 0.94 \log_{10} M_2 - 1.52 \log_{10} v_{-1} + 2.02 \log_{10} \kappa_{10}$$
$$m_z = -12.80 - 0.94 \log_{10} M_2 - 1.56 \log_{10} v_{-1} + 1.87 \log_{10} \kappa_{10}$$
$$m_y = -12.90 - 0.93 \log_{10} M_2 - 1.61 \log_{10} v_{-1} + 1.76 \log_{10} \kappa_{10}$$
$$m_J = -13.14 - 0.93 \log_{10} M_2 - 1.61 \log_{10} v_{-1} + 1.56 \log_{10} \kappa_{10}$$
$$m_H = -13.33 - 0.95 \log_{10} M_2 - 1.55 \log_{10} v_{-1} + 1.33 \log_{10} \kappa_{10}$$
$$m_K = -13.44 - 0.99 \log_{10} M_2 - 1.53 \log_{10} v_{-1} + 1.13 \log_{10} \kappa_{10}$$

$$t_\mathrm{p} = 1.87\ \mathrm{d}\ M_2^{0.365}\ v_{-1}^{-0.551}\ \kappa_{10}^{0.34}$$

$$L_\mathrm{p} = 1.4 \times 10^{40}\ \mathrm{erg\ s^{-1}}\ M_2^{0.393}\ v_{-1}^{0.618}\ \kappa_{10}^{-0.59}$$

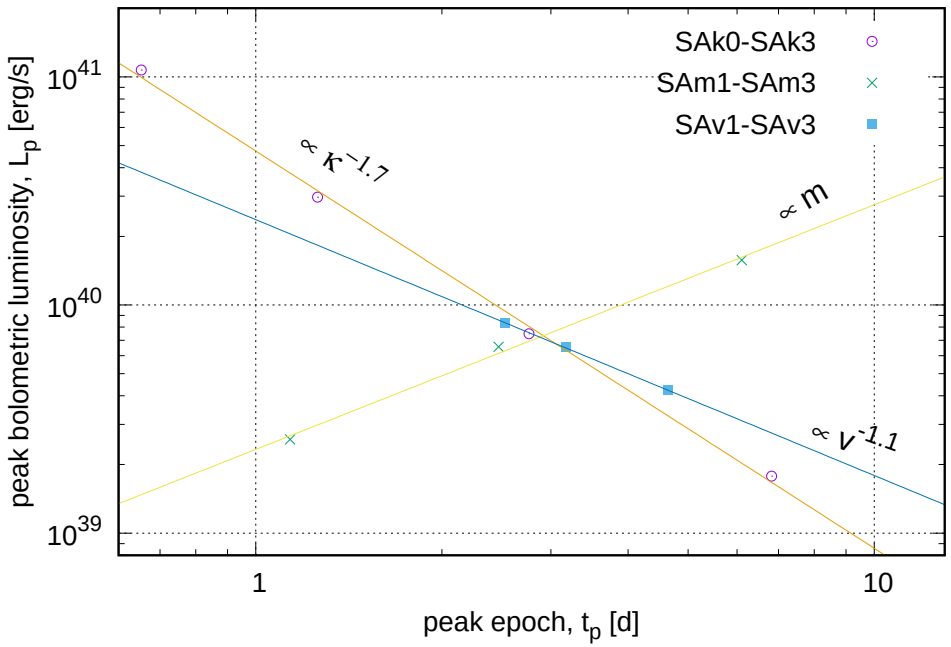

Dynamical ejecta (2D)

- Rosswog et al (2013):
  - A ($M = .013\ \mathrm{M}_\odot$),
  - B ($M = .014\ \mathrm{M}_\odot$),
  - C ($M = .033\ \mathrm{M}_\odot$),
  - D ($M = .034\ \mathrm{M}_\odot$).
- 2D cylindrical geometry.
- Heating rate is analytic (as in 1D).
- Sm opacity.

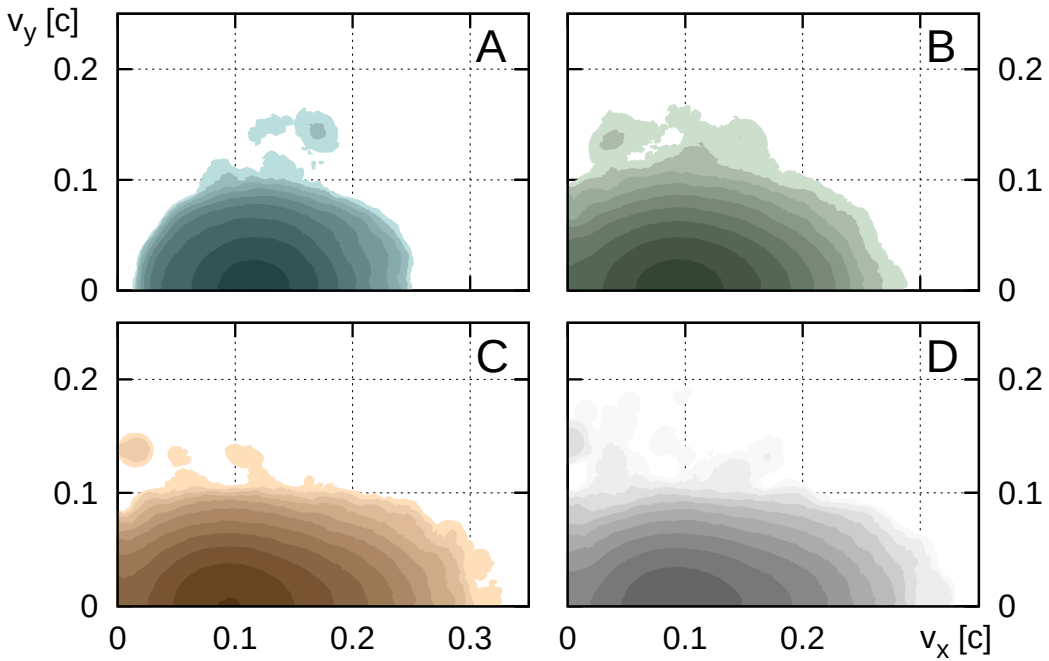

Dynamical ejecta (2D)

- View along axis (top):

Peak magnitude, m								
Model	g	r	i	z	y	J	H	K
A2dSm	-6.7	-7.9	-9.4	-9.8	-10.1	-10.9	-13.3	-14.5
B2dSm	-6.0	-8.5	-9.5	-10.0	-10.4	-11.0	-13.4	-14.6
C2dSm	-6.2	-8.1	-10.0	-10.5	-10.8	-11.4	-13.9	-15.2
D2dSm	-6.1	-8.7	-10.2	-10.6	-10.9	-11.5	-14.0	-15.2

Peak epoch, t_p [d]								
Model	g	r	i	z	y	J	H	K
A2dSm	0.35	0	0	0	0	0.38	4.47	5.22
B2dSm	0	0	0	0	0	0.33	4.37	5.30
C2dSm	0	0	0	0	0.29	0.47	4.98	6.48
D2dSm	0.26	0.28	0	0	0.26	0.45	5.20	6.47

Dynamical ejecta (2D)

- View along axis (top):

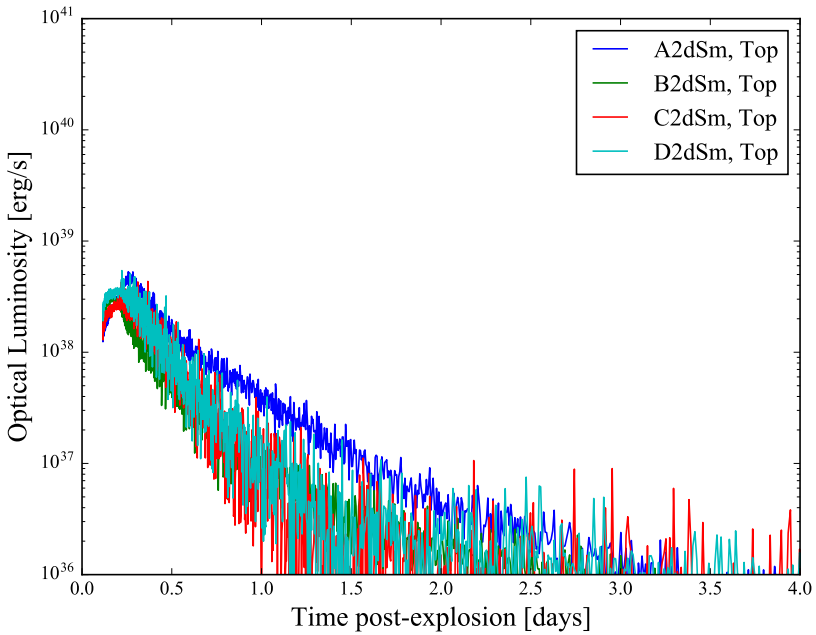

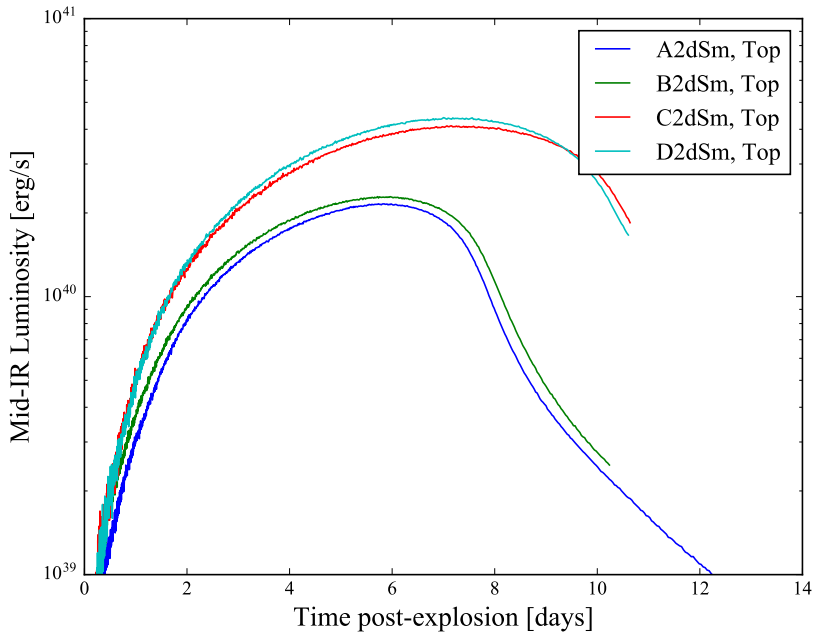

Dynamical ejecta (2D)

- View in equatorial plane (side):

Peak magnitude, m								
Model	g	r	i	z	y	J	H	K
A2dSm	-6.3	-8.8	-9.9	-10.2	-10.5	-11.4	-13.1	-13.9
B2dSm	-6.7	-8.9	-9.7	-10.2	-10.5	-11.5	-13.2	-13.9
C2dSm	-7.3	-9.6	-10.2	-10.5	-10.7	-11.8	-13.6	-14.3
D2dSm	-7.4	-9.6	-10.3	-10.8	-10.9	-12.0	-13.8	-14.4

Peak epoch, t_p [d]								
Model	g	r	i	z	y	J	H	K
A2dSm	0.30	0	0	0	0.28	0.48	3.33	4.82
B2dSm	0	0	0	0	0	0.49	2.57	4.81
C2dSm	0	0	0	0	0	1.44	3.36	6.26
D2dSm	0	0	0	0.27	0.30	1.34	3.30	5.97

Dynamical ejecta (2D)

- View in equatorial plane (side):

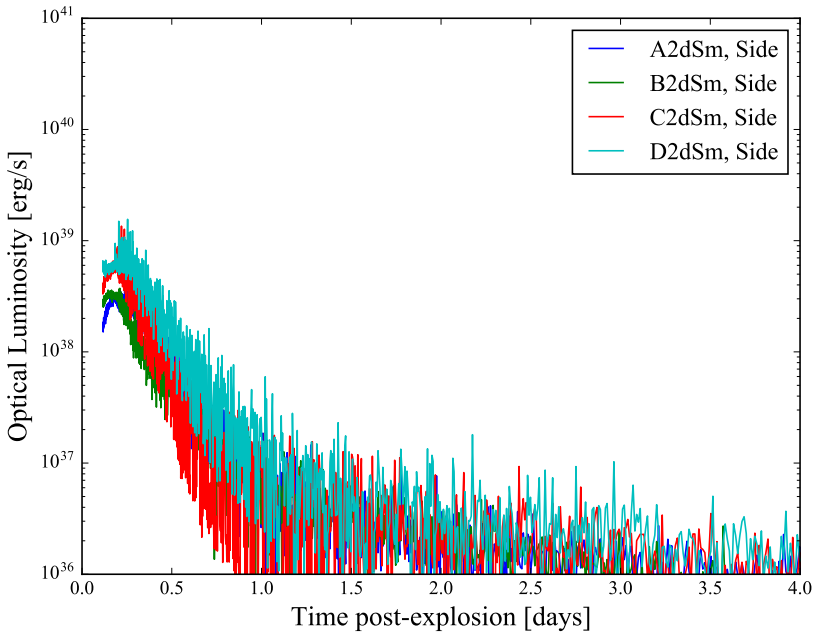

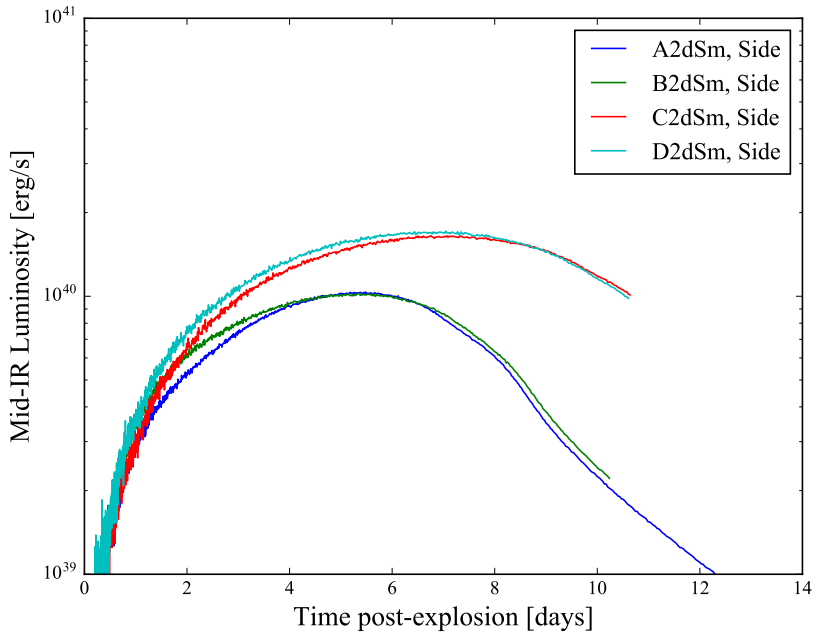

Dynamical ejecta + wind (2D)

- Models A-D have superimposed spherically symmetric analytic wind ($V_{\max} = .16c$, $M = .005\ \mathrm{M}_{\odot}$).
- 2D cylindrical geometry.
- Heating rate is analytic (as in 1D).
- Sm opacity for dyn. ej., Zr opacity for wind.
- Opacity is mass fraction weighted.

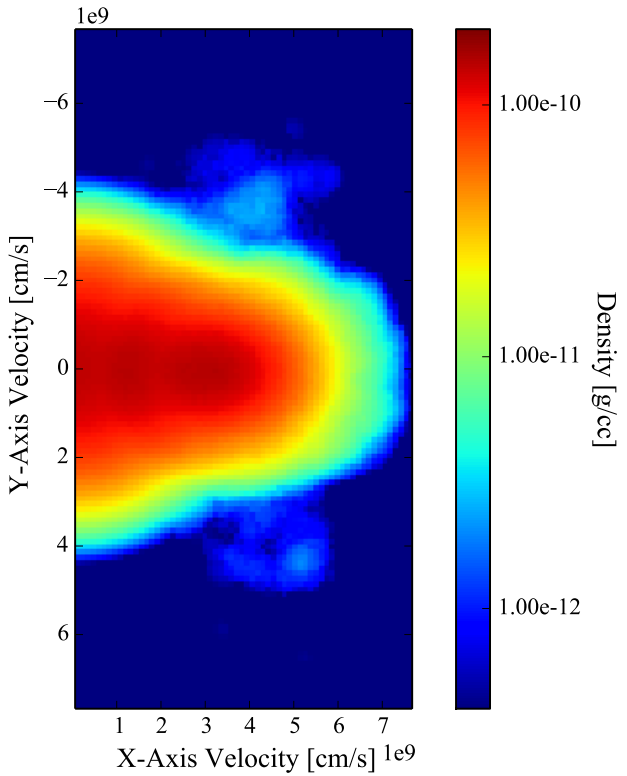

Dynamical ejecta + wind (2D)

- View along axis (top):

Peak magnitude, m								
Model	g	r	i	z	y	J	H	K
W2A	-12.1	-12.0	-12.3	-12.4	-12.3	-12.5	-13.9	-14.6
W2B	-6.0	-8.5	-9.5	-10.0	-10.3	-11.1	-13.8	-14.6
W2C	-11.6	-11.4	-11.9	-12.1	-12.2	-12.5	-14.2	-15.2
W2D	-7.2	-9.1	-10.5	-11.0	-11.3	-11.7	-14.2	-15.3

Peak epoch, t_p [d]								
Model	g	r	i	z	y	J	H	K
W2A	0.45	0.61	0.69	0.79	0.74	0.92	2.64	6.23
W2B	0	0	0	0	0	0.34	4.70	5.77
W2C	0.37	0.43	0.47	0.40	0.41	0.59	4.83	6.98
W2D	0.33	0.32	0.35	0.33	0.36	0.46	5.07	6.85

Dynamical ejecta + wind (2D)

- View along axis (top):

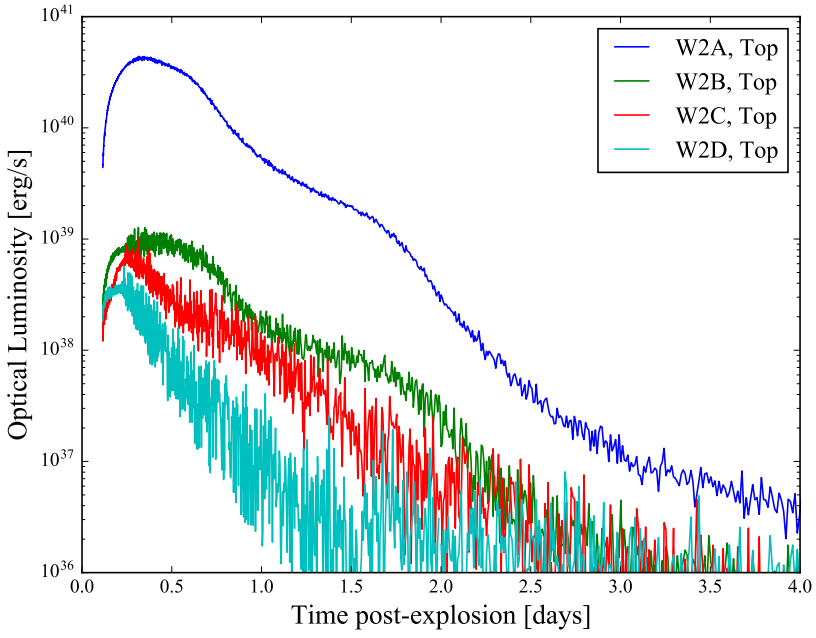

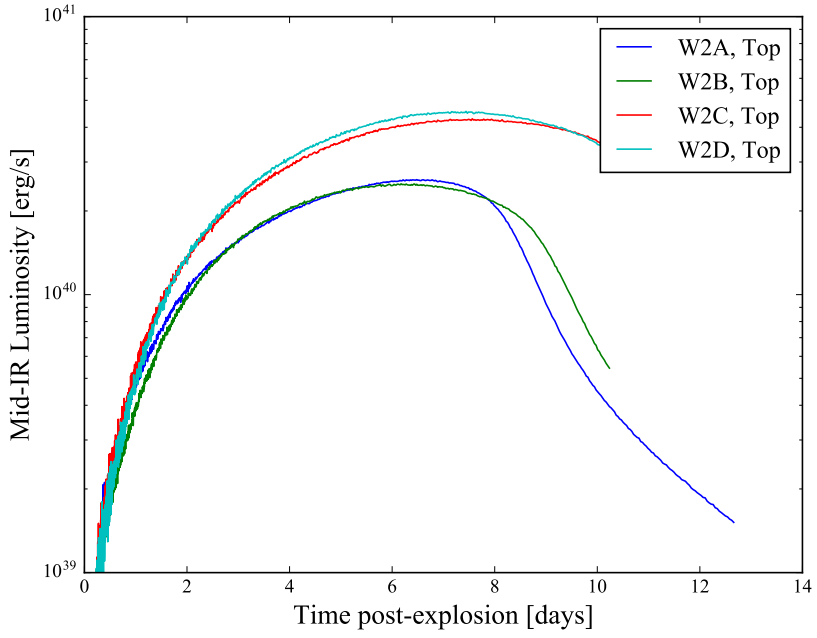

Dynamical ejecta + wind (2D)

- View in equatorial plane (side):

Peak magnitude, m								
Model	g	r	i	z	y	J	H	K
W2A	-6.2	-8.8	-9.9	-10.2	-10.6	-11.4	-13.2	-14.0
W2B	-6.7	-9.0	-9.8	-10.2	-10.5	-11.4	-13.2	-14.0
W2C	-7.2	-9.6	-10.2	-10.5	-10.6	-11.8	-13.6	-14.4
W2D	-7.4	-9.6	-10.3	-10.8	-11.0	-12.0	-13.8	-14.5

Peak epoch, t_p [d]								
Model	g	r	i	z	y	J	H	K
W2A	0.29	0	0	0	0.30	0.48	3.16	5.31
W2B	0	0	0	0	0	0.52	2.52	5.14
W2C	0	0	0	0	0	1.38	3.32	6.49
W2D	0	0	0	0.27	0.31	1.51	3.45	5.98

Dynamical ejecta + wind (2D)

- View in equatorial plane (side):

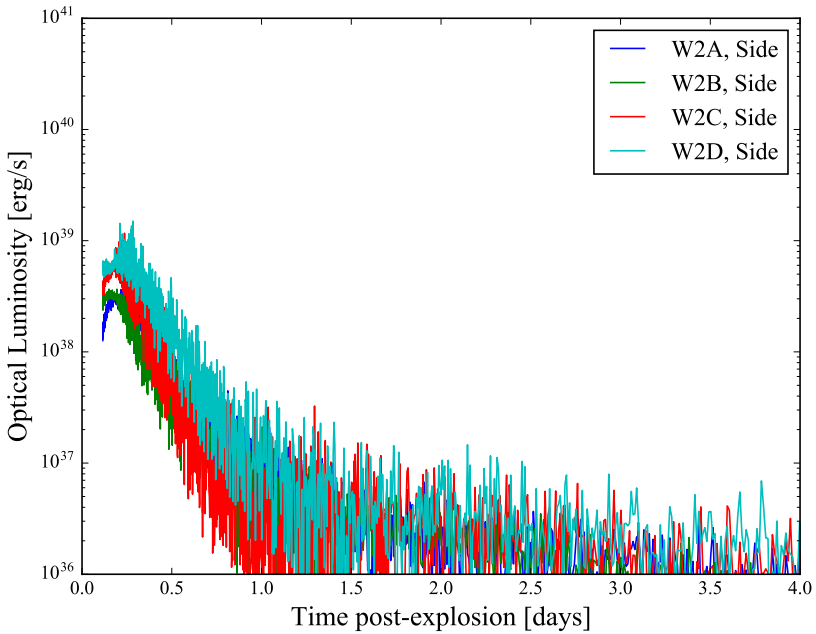

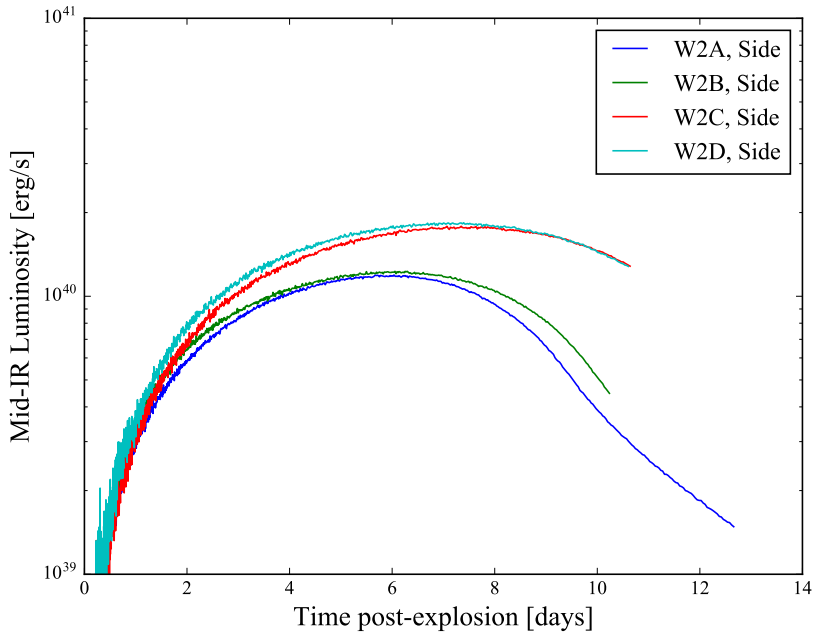

More realistic models (2D)

- Dyn. ej. and wind compositions are reduced from r-process distributions from NSM tracer particles. (Perego et al 2014)
- Opacities are mass-fraction weighted.
- r-process heating from WinNet and thermalization fractions from Barnes et al (2016) (Winteler 2011 PhD thesis, Barnes et al 2016)
- Grey absorption opacity for γ-ray thermalization and simplified MC transport is set to 0.1 cm^2/g.

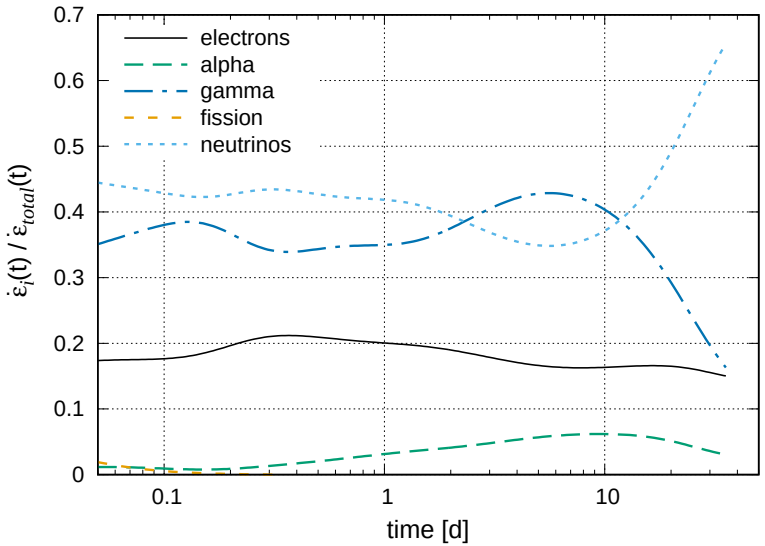

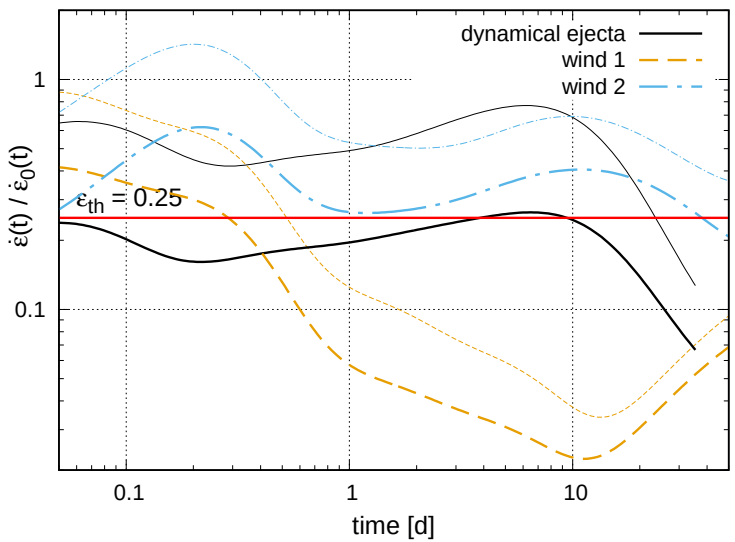

More realistic models (2D)

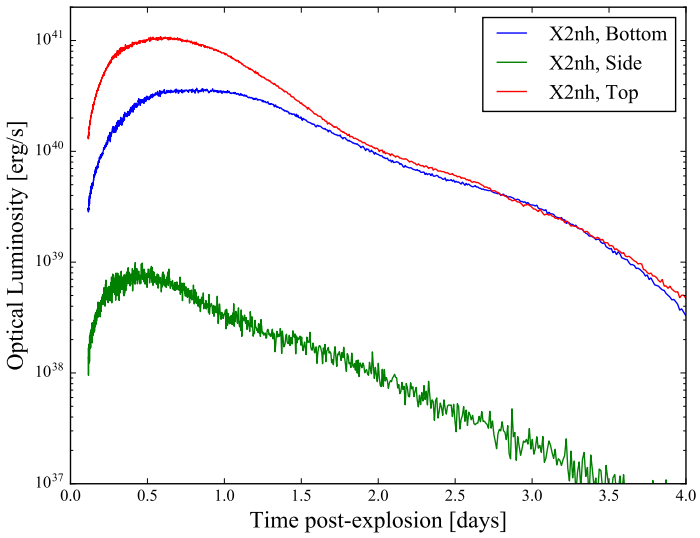

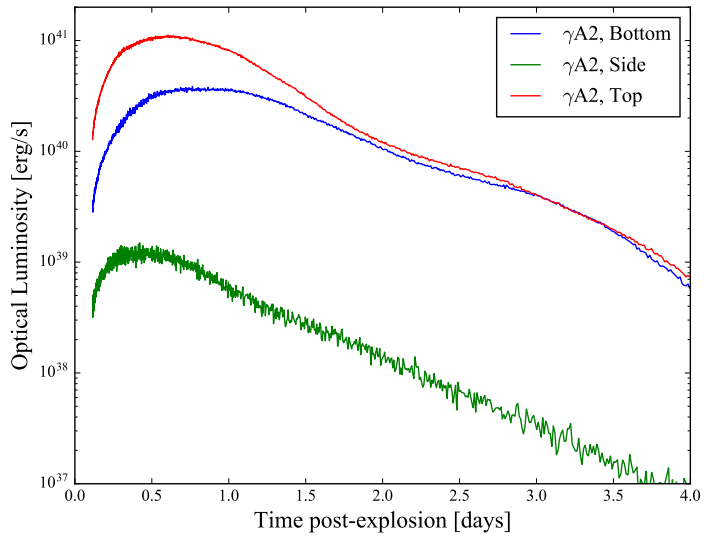

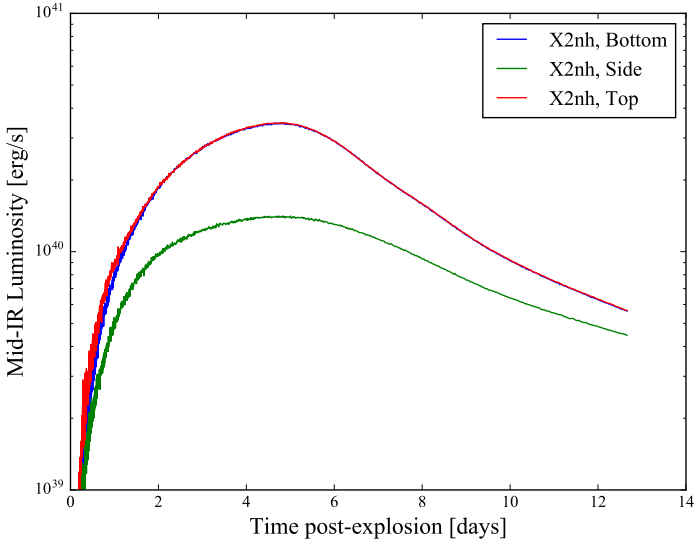

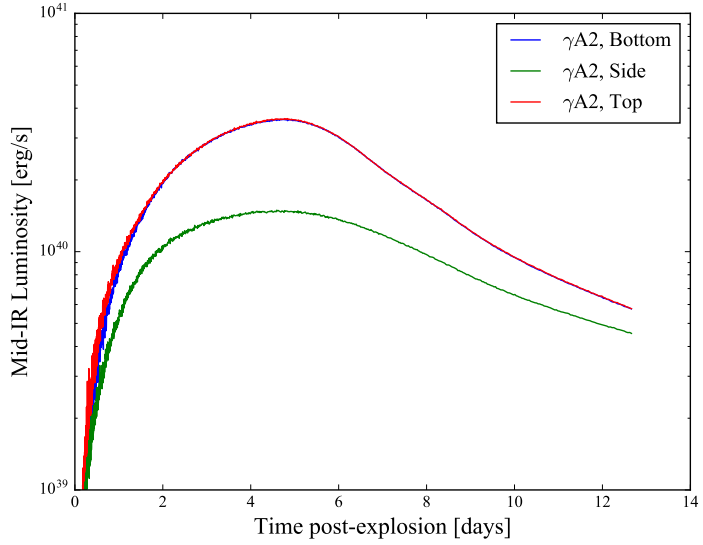

Conclusions

- `SuperNu` and the LANL suite of atomic physics codes have been applied to model light curves for macronovae/kilonovae.
- Rosswog et al (2013) models A-D have been used for the dynamical ejecta, with a spherically symmetric wind superimposed.
- Light curves are on the order of a few days in the IR bands.
- The optical bands and luminosity are typically dim, and optical transients from the wind are sensitive to dynamical ejecta mixing.
- Absolute peak K-band magnitudes range from -11 to -15, more realistic models range from -14 to -15.

Thank You!

References I

D Argast, Ma Samland, F-K Thielemann, and Y-Z Qian.
Neutron star mergers versus core-collapse supernovae as dominant r-process sites in the early galaxy.
Astronomy & Astrophysics, 416(3):997–1011, 2004.

J Barnes, D Kasen, M Wu, and G Mart'inez-Pinedo.
Radioactivity and thermalization in the ejecta of compact object mergers and their impact on kilonova light curves.
arXiv preprint arXiv:1605.07218, 2016.

B Côté, K Belczynski, CL Fryer, C Ritter, A Paul, B Wehmeyer, and BW O'Shea.
Advanced ligo constraints on neutron star mergers and r-process sites.
arXiv preprint arXiv:1610.02405, 2016.

S Dado and A Dar.
Grb 130603b: No compelling evidence for neutron star merger.
Advances in Astronomy, 2015, 2015.

W Fong, E Berger, R Margutti, and BA Zauderer.
A decade of short-duration gamma-ray burst broadband afterglows: Energetics, circumburst densities, and jet opening angles.
The Astrophysical Journal, 815(2):102, 2015.

W Fong, R Margutti, R Chornock, E Berger, BJ Shappee, AJ Levan, NR Tanvir, N Smith, PA Milne, T Laskar, et al.
The afterglow and early-type host galaxy of the short grb 150101b at z= 0.1343.
The Astrophysical Journal, 833(2):151, 2016.

CJ Fontes, CL Fryer, AL Hungerford, P Hakel, J Colgan, DP Kilcrease, and ME Sherrill.
Relativistic opacities for astrophysical applications.
High Energy Density Physics, 16:53–59, 2015.

CJ Fontes, HL Zhang, J Abdallah Jr, REH Clark, DP Kilcrease, J Colgan, RT Cunningham, P Hakel, NH Magee, and ME Sherrill.
The Los Alamos suite of relativistic atomic physics codes.
Journal of Physics B: Atomic, Molecular and Optical Physics, 48(14):144014, 2015.

References II

CL Fryer, K Belczynski, E Ramirez-Ruiz, S Rosswog, G Shen, and AW Steiner.
The fate of the compact remnant in neutron star mergers.
The Astrophysical Journal, 812(1):24, 2015.

CL Fryer, SE Woosley, and DH Hartmann.
Formation rates of black hole accretion disk gamma-ray bursts.
The Astrophysical Journal, 526(1):152, 1999.

K Hotokezaka, T Piran, and M Paul.
Short-lived ^{244}Pu points to compact binary mergers as sites for heavy r-process nucleosynthesis.
arXiv preprint arXiv:1510.00711, 2015.

AP Ji, A Frebel, A Chiti, and JD Simon.
R-process enrichment from a single event in an ancient dwarf galaxy.
Nature, 2016.

O Korobkin, S Rosswog, A Arcones, and C Winteler.
On the astrophysical robustness of the neutron star merger r-process.
Monthly Notices of the Royal Astronomical Society, 426(3):1940–1949, 2012.

P Lazarus, PCC Freire, B Allen, C Aulbert, O Bock, S Bogdanov, A Brazier, F Camilo, F Cardoso, S Chatterjee, et al.
Einstein@ home discovery of a double neutron star binary in the palfa survey.
The Astrophysical Journal, 831(2):150, 2016.

L Li and B Paczyński.
Transient events from neutron star mergers.
The Astrophysical Journal Letters, 507(1):L59, 1998.

D Martin, A Perego, A Arcones, F-K Thielemann, O Korobkin, and S Rosswog.
Neutrino-driven winds in the aftermath of a neutron star merger: nucleosynthesis and electromagnetic transients.
The Astrophysical Journal, 813(1):2, 2015.

References III

JG Martinez, K Stovall, PCC Freire, JS Deneva, FA Jenet, MA McLaughlin, M Bagchi, SD Bates, and A Ridolfi.
Pulsar j0453+ 1559: A double neutron star system with a large mass asymmetry.
The Astrophysical Journal, 812(2):143, 2015.

BD Metzger.
The kilonova handbook.
arXiv preprint arXiv:1610.09381, 2016.

BD Metzger, G Martínez-Pinedo, S Darbha, E Quataert, A Arcones, D Kasen, R Thomas, P Nugent, IV Panov, and Nikolaj Thomas Zinner.
Electromagnetic counterparts of compact object mergers powered by the radioactive decay of r-process nuclei.
Monthly Notices of the Royal Astronomical Society, 406(4):2650–2662, 2010.

F Özel and P Freire.
Masses, radii, and equation of state of neutron stars.
arXiv preprint arXiv:1603.02698, 2016.

A Perego, S Rosswog, RM Cabezón, O Korobkin, R Kaeppeli, A Arcones, and M Liebendoerfer.
Neutrino-driven winds from neutron star merger remnants.
Monthly Notices of the Royal Astronomical Society, 443(4):3134–3156, 2014.

S Rosswog, O Korobkin, A Arcones, F-K Thielemann, and T Piran.
The long-term evolution of neutron star merger remnants–i. the impact of r-process nucleosynthesis.
Monthly Notices of the Royal Astronomical Society, 439(1):744–756, 2014.

S Rosswog, T Piran, and E Nakar.
The multimessenger picture of compact object encounters: binary mergers versus dynamical collisions.
Monthly Notices of the Royal Astronomical Society, page sts708, 2013.

C Sneden, JJ Cowan, and R Gallino.
Neutron-capture elements in the early galaxy.
Annu. Rev. Astron. Astrophys., 46:241–288, 2008.

References IV

NR Tanvir, AJ Levan, AS Fruchter, J Hjorth, RA Hounsell, K Wiersema, and RL Tunnicliffe.
A/kilonova/'associated with the short-duration [ggr]-ray burst grb [thinsp] 130603b.
Nature, 2013.

A Wallner, T Faestermann, J Feige, C Feldstein, K Knie, G Korschinek, W Kutschera, A Ofan, M Paul, F Quinto, et al.
Abundance of live 244Pu in deep-sea reservoirs on earth points to rarity of actinide nucleosynthesis.
Nature communications, 6, 2015.

JM Weisberg, DJ Nice, and JH Taylor.
Timing measurements of the relativistic binary pulsar psr b1913+ 16.
The Astrophysical Journal, 722(2):1030, 2010.

RT Wollaeger and DR Van Rossum.
Radiation transport for explosive outflows: Opacity regrouping.
The Astrophysical Journal Supplement Series, 214(2):28, 2014.

RT Wollaeger, DR van Rossum, C Graziani, SM Couch, GC Jordan IV, DQ Lamb, and GA Moses.
Radiation transport for explosive outflows: A multigroup hybrid monte carlo method.
The Astrophysical Journal Supplement Series, 209(2):36, 2013.

B Yang, Z Jin, X Li, S Covino, X Zheng, K Hotokezaka, Y Fan, T Piran, and D Wei.
A possible macronova in the late afterglow of the long-short burst grb 060614.
Nature communications, 6, 2015.